ADVANCING EARTH AND SPACE SCIENCES

Geophysical Research Letters

RESEARCH LETTER

10.1029/2023GL107825

Key Points:

- Low-frequency hiss waves were excited by energetic electrons inside the dayside plasmaspheric plume following substorms
- Low-frequency hiss rays survived at least 42 s, allowing themselves to migrate from the plasmaspheric plume to the plasmaspheric core
- Plasmaspheric density ducts facilitated the permeation of hiss rays from the plasmaspheric plume to the plasmaspheric core

Supporting Information:

Supporting Information may be found in the online version of this article.

Correspondence to:

Z. Su,
szpe@mail.ustc.edu.cn

Citation:

Wu, Z., Su, Z., Zheng, H., Wang, Y., Miyoshi, Y., Shinohara, I., et al. (2024). Long lifetime hiss rays in the disturbed plasmasphere. *Geophysical Research Letters*, *51*, e2023GL107825. https://doi.org/10.1029/2023GL107825

Received 12 DEC 2023
Accepted 6 FEB 2024

Long Lifetime Hiss Rays in the Disturbed Plasmasphere

Zhiyong Wu[1,2,3], Zhenpeng Su[1,2,3], Huinan Zheng[1,2,3], Yuming Wang[1,2,3], Yoshizumi Miyoshi[4], Iku Shinohara[5], Ayako Matsuoka[6], Yoshiya Kasahara[7], Fuminori Tsuchiya[8], Atsushi Kumamoto[8], Shoya Matsuda[7], Yasumasa Kasaba[8], Mariko Teramoto[9], and Tomoaki Hori[4]

[1]Deep Space Exploration Laboratory/School of Earth and Space Sciences, University of Science and Technology of China, Hefei, China, [2]CAS Center for Excellence in Comparative Planetology/CAS Key Laboratory of Geospace Environment/Mengcheng National Geophysical Observatory, University of Science and Technology of China, Hefei, China, [3]Collaborative Innovation Center of Astronautical Science and Technology, Harbin, China, [4]Institute for Space-Earth Environmental Research, Nagoya University, Nagoya, Japan, [5]Institute of Space and Astronautical Science, Japan Aerospace Exploration Agency, Sagamihara, Japan, [6]Graduate School of Science, Kyoto University, Kyoto, Japan, [7]Graduate School of Natural Science and Technology, Kanazawa University, Kanazawa, Japan, [8]Graduate School of Science, Tohoku University, Sendai, Japan, [9]Graduate School of Engineering, Kyushu Institute of Technology, Kitakyushu, Japan

Abstract Plasmaspheric hiss waves are important to shape the Earth's electron radiation belt. These waves are commonly envisioned to have a long lifetime which allows them to permeate the global plasmasphere from a spatially restricted source. However, this hypothesis has not been experimentally confirmed yet, because of the challenging observational requirements in terms of location and timing. With wave and particle measurements from five magnetospheric satellites and detailed modeling, we present the first report of long lifetime (∼42 s) hiss rays in the substorm-disturbed plasmasphere. The low-frequency hiss waves are found to originate from the middle piece of the plasmaspheric plume, bounce between two hemispheres, and eventually drift into the plasmaspheric core. These hiss rays can travel through ∼3 hr magnetic local time and ∼4 magnetic shell. Such a long-time and large-scale permeation of hiss rays could benefit from the ducting process by plasmaspheric field-aligned density irregularities.

Plain Language Summary Earth's plasmasphere is populated by a type of whistler-mode wave named plasmaspheric hiss which is able to shape the electron radiation belt. Hiss waves were commonly envisioned to have a long lifetime which allows them to permeate the global plasmasphere from a spatially restricted source. Although there have been numerous studies on the source of plasmaspheric hiss waves, the hypothesis regarding their long lifetime remains not experimentally confirmed yet because of the challenging observational requirements in terms of location and timing. On the basis of wave and particle measurements from five magnetospheric satellites covering the entire plasmasphere and detailed modeling, we show that the hiss rays can survive at least 42 s in the plasmasphere disturbed by substorms. Within the survival period, these hiss rays migrated from the middle piece of the plasmaspheric plume to the plasmaspheric core, whose path lengths reached 25 Earth radii. Such a long-time and large-scale permeation of hiss rays from the plasmaspheric plume to the plasmaspheric core could benefit from the ducting process by plasmaspheric field-aligned density irregularities.

1. Introduction

The Earth's plasmasphere is populated by a type of whistler-mode wave named plasmaspheric hiss (Chan & Holzer, 1976; Dunckel & Helliwell, 1969; Meredith et al., 2004; Ni et al., 2023; Russell et al., 1969; Su et al., 2018a; Thorne et al., 1973; Tsurutani et al., 2015; Yang et al., 2022; Yu et al., 2017). Plasmaspheric hiss waves have been well known to scatter the radiation belt electrons (Li et al., 2007; Summers et al., 2008; Shprits, 2009; Ni et al., 2013; Breneman et al., 2015; Zhang et al., 2019; Fu et al., 2020), causing the slot region separating the inner and outer radiation belts (Abel & Thorne, 1998; Lyons et al., 1972; Lyons & Thorne, 1973), the slow decay of radiation belts (Thorne et al., 2013; Xiao et al., 2009), and the reversed energy spectrum of electrons (Ni et al., 2019; Zhao et al., 2019). These waves are commonly envisioned to have a spatially restricted source but survive long to permeate the global plasmasphere (Chen et al., 2009; Liu et al., 2020; Santolík et al., 2021; Su et al., 2018b; Thorne et al., 1973; Wu et al., 2022). Three types of sources for plasmaspheric hiss

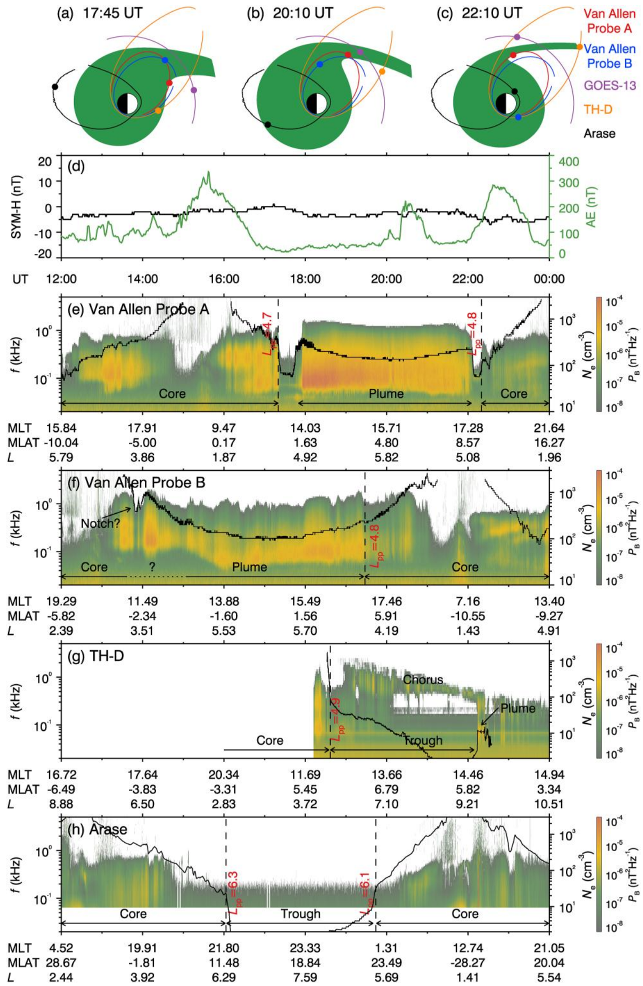

Figure 1. Overview of plasmaspheric morphology and hiss waves on 03 July 2017. (a)–(c) Schematic diagrams of plasmasphere morphology, overlain by the orbits (solid lines) and locations at specific moments (solid dots) of Van Allen Probes A and B, TH-D, Arase, and GOES-13. (d) Geomagnetic indices SYM-H (black) and AE (green). Wave magnetic power spectral densities P_B (color-coded) from (e) Van Allen Probes A and (f) B, (g) TH-D, and (h) Arase, overlain by electron densities N_e (black lines).

have been proposed and verified: (a) lightning-generated whistler waves in low-altitude atmosphere (Green et al., 2020; Meredith et al., 2006; Sonwalkar & Inan, 1989); (b) whistler-mode chorus waves outside the plasmasphere (Bortnik et al., 2008; Bortnik et al., 2009; Wang et al., 2011; Meredith et al., 2013; Li et al., 2015; Zhou et al., 2016); (c) background thermal noises amplified by energetic electrons in the outer core or plume of the plasmasphere (Thorne et al., 1973; Li et al., 2013; Chen et al., 2014; Laakso et al., 2015; Su et al., 2018a, Su et al., 2018b). In contrast, the hypothesis of a long lifetime of hiss rays remains not experimentally confirmed yet.

The lifetime of hiss rays may be determined by three types of physical processes: (a) Landau damping by suprathermal electrons (Thorne & Horne, 1994; Zhu et al., 2015; Li et al., 2019; Wang et al., 2020); (b) cyclotron absorption by thermal ions at low altitudes (Chen et al., 2020; Kintner et al., 1991); (c) energy bifurcation at the wavelength-scale density irregularities (Woodroffe & Streltsov, 2014; Zudin et al., 2019). On the basis of Wentzel-Kramer-Brillouin (WKB) approximation, several ray-tracing simulations with Landau damping alone suggest a lifetime of 100 s for plasmaspheric hiss (Bortnik et al., 2003, 2008, 2011; Chen et al., 2009). To what extent the other two processes affect the lifetime of hiss rays has not been evaluated systematically. In experiment, to identify the hiss rays with a lifetime on the order of 100 s is challenging. First, two spacecraft are required to be located on the path of hiss propagation. Second, the hiss waves are required to exhibit some frequency-time structures to allow cross-spacecraft tracing.

In this letter, with five magnetospheric spacecraft, Van Allen Probes A and B (Mauk et al., 2013), TH-D of the Time History of Events and Macroscale Interactions during Substorms (THEMIS) mission (Angelopoulos, 2008), GOES-13 of the Geostationary Operational Environmental Satellites (GOES) mission (Davis, 2007), and Arase (also known as the Exploration of energization and Radiation in Geospace, ERG) (Miyoshi et al., 2022; Miyoshi, Shinohara, Takashima, et al., 2018), we investigate the evolution of plasmasphere and the generation and propagation of plasmaspheric hiss waves following a series of substorms on 03 July 2017. These hiss waves happened to be modulated by an ultralow-frequency magnetic perturbation, allowing the cross-spacecraft tracing. The significant lag-correlation between low-frequency hiss waves in the plasmaspheric core and in the near-base piece of the plasmaspheric plume supports the propagation of waves between the two places within 27 s. The wave Poynting flux measurements, linear growth rate calculations, and ray-tracing simulations further establish the hiss wave source in the middle piece of the plasmaspheric plume. Our data and modeling together demonstrate that hiss rays in the disturbed plasmasphere probably survived at least 42 s.

2. Event Overview

As depicted in Figures 1a–1c, the enhanced magnetospheric convection related to substorms (Figure 1d) caused the formation of plasmaspheric plume drained from the plasmaspheric core on 03 July 2017. These boundaries of the plasmaspheric core and plume are determined on the basis of density and wave measurements from four magnetospheric spacecraft (Figures 1e–1h): Van Allen Probes, TH-D, and Arase. For Van Allen Probes and Arase, the electron density is derived from the upper hybrid frequency (Kurth et al., 2015) which was measured by the High Frequency Receiver (HFR) of the Electric and Magnetic Field Instrument and Integrated Science (EMFISIS) suite (Kletzing et al., 2013) and the High-Frequency Analyzer (HFA; Kumamoto et al., 2018) of Plasma Wave Experiment (PWE; Kasahara et al., 2018), respectively. For TH-D, the electron density is estimated from the spacecraft potential (Nishimura et al., 2013) which was measured by the Electrostatic Analyzer (ESA; McFadden et al., 2008). The wave power spectral density was measured by the Waveform Receiver (WFR) of

EMFISIS, the Search Coil Magnetometer (SCM; Roux et al., 2008), and the Onboard Frequency Analyzer (OFA; Matsuda et al., 2018) of PWE for the three missions, respectively.

For Van Allen Probe A (Figure 1e) and TH-D (Figure 1g) on the dayside, the density jumps closer to Earth signified the passages through the plasmaspheric core boundary (plasmapause), and the density jumps further away from Earth signified the passages through the plasmaspheric plume boundary. For Arase (Figure 1h) on the nightside, only the density jumps related to the plasmapause existed. The plasmapause was located around $L = 4.8$ on the dayside and $L = 6.1$ on the nightside. The dayside plasmaspheric plume extended to at least $L = 9.2$ (TH-D). The plasmaspheric hiss was strongest in the dayside plasmaspheric plume, followed by the pre-noon plasmaspheric core, weaker in the duskside plasmaspheric core, and weakest in the nightside plasmaspheric core. Nearly in the same orbit as Van Allen Probe A, Probe B gave a quite different density profile during 13:30–21:15 UT (Figure 1f). Van Allen Probe B probably crossed a notch (Gallagher et al., 2005) at 13:50 UT ($L = 3.2$) and then persisted in the high-density environment during the next 7 hr. A reasonable explanation is that, along with the evolution and rotation of the plasmasphere, Van Allen Probe B moved from the core through the plume's base to the plume and re-entered the core through the plume's base. The duskside plume-to-core boundary may be characterized by the jump of plasmaspheric hiss power at 19:30 UT, whose location was generally consistent with the plasmapause observations of Van Allen Probe A and TH-D at the nearest moments.

Figure 2a presents the perturbations in the magnetic field magnitude from 20:00 UT to 20:20 UT, measured by the tri-axial fluxgate Magnetometer (MAG) of EMFISIS suite onboard Van Allen Probes, the three orthogonal fluxgate magnetometer elements (MAG) onboard GOES, the Fluxgate Magnetometer (FGM; Auster et al., 2008) onboard THEMIS, and the Magnetic Field Experiment (MGF; Matsuoka, Teramoto, Nomura, et al., 2018) onboard Arase. The magnetic field perturbations are calculated by subtracting the 8-min running average of magnetic field magnitude from the instantaneous magnetic field magnitude. The spatial locations of the five spacecraft with respect to the plasmasphere have been described in Figure 1b. Van Allen Probe A ($L \sim 5.8$ and MLT ~ 15.8), GOES-13 ($L \sim 6.8$ and MLT ~ 15.3) and TH-D ($L \sim 7.3$ and MLT ~ 13.7) on the noonside simultaneously observed the spatially coherent magnetic field perturbation which was unobservable for Van Allen Probe B ($L \sim 4.1$ and MLT ~ 17.7) on the duskside and Arase ($L \sim 5.7$ and MLT ~ 1.5) on the nightside (Figure 2a). This magnetic field perturbation had a peak-to-peak amplitude of 2–2.5 nT and a period of ~8 min. As shown in Figure 2b, the electron densities behaved in different ways from the magnetic fields, indicating the absence of density fluctuations related to the ultralow-frequency magnetic perturbations. These high-resolution electron densities estimated from the spacecraft potentials measured by the Electric Field and Wave (EFW; Wygant et al., 2013) onboard Van Allen Probes, the Electrostatic Analyzer (ESA; McFadden et al., 2008) onboard THEMIS, and the Electric Field Detector (EFD; Kasaba et al., 2017) of the Plasma Wave Experiment (PWE; Kasahara et al., 2018) onboard Arase. Following the work of Kazama et al. (2018), the electron density N_e and spacecraft potential U are related as

$$N_e = C_1 e^{C_2 U} \tag{1}$$

with fitting parameters $C_1 = 198.93\ \text{cm}^{-3}$ and $C_2 = 0.29\ \text{V}^{-1}$ for Van Allen Probe A; $C_1 = 8{,}212.31\ \text{cm}^{-3}$ and $C_2 = 4.59\ \text{V}^{-1}$ for Van Allen Probe B; $C_1 = 176.15\ \text{cm}^{-3}$ and $C_2 = 2.73\ \text{V}^{-1}$ for Arase. As for TH-D, the specific technique was developed by Nishimura et al. (2013).

Interestingly, Van Allen Probe A observed plasmaspheric hiss waves seemingly modulated by the weak magnetic perturbation (Figure 2c). At Van Allen Probe B without the magnetic perturbation, the plasmaspheric hiss waves still exhibited a similar modulation feature (Figure 2d). From Probe A to Probe B, the power spectral density of hiss waves decreased by approximately one order of magnitude (Figures 2c–2e). When the low-frequency (80–112 Hz) hiss waves of Probe B lag behind those of Probe A by 15–33 s, their cross-correlation becomes significant. Particularly, the peak correlation coefficient $r_{AB} = 0.6$ occurs at the time lag of 27 s for the hiss waves of 90 Hz. These results indicate that the propagation of low-frequency hiss rays from the near-base piece of the plasmaspheric plume to the plasmaspheric core. In other words, the 90 Hz hiss rays had survived at least 27 s, which is approximately 4–5 times larger than previous direct measurements of hiss ray lifetimes (Bortnik et al., 2009; Wang et al., 2011; Li et al., 2015; Wu et al., 2022). The cross-correlation of low-frequency hiss waves exhibits some dispersion over the lag time, which may be caused by noise contamination on the low-resolution (6 s) wave data or superposition of waves with different propagation times. At higher frequencies, the detected wave power was weaker and consequently the results from the cross-correlation analysis may become less reliable.

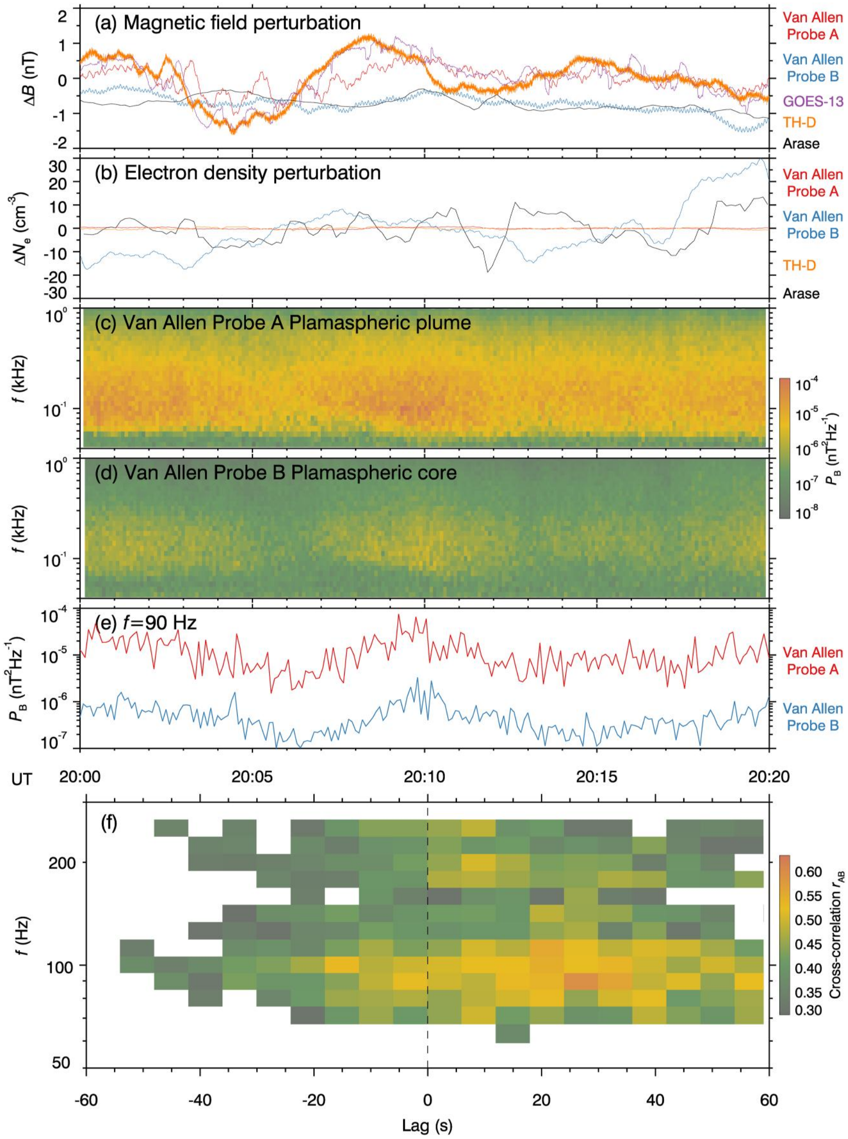

Figure 2. Cross-correlation analysis between hiss signals from Van Allen Probes A and B during 20:00–20:20 UT. (a) Perturbations ΔB of magnetic field magnitudes from five magnetospheric spacecraft (indicated). ΔB is calculated by subtracting the 8-min running average of magnetic field magnitude from the instantaneous magnetic field magnitude. (b) Electron density perturbations ΔN_e calculated in the same way as that of ΔB calculation. Wave magnetic power spectral densities P_B observed by (c) Van Allen Probes A and (d) B. (e) Wave magnetic power spectral density profiles P_B at $f = 90$ Hz from Van Allen Probes A (red) and B (blue). (f) Cross-correlation coefficients r_{AB} of wave magnetic power spectral densities between Van Allen Probes A and B. Positive (negative) time lags represent the lagging (leading) of signals of Probe B against those of Probe A.

3. Generation of Plasmaspheric Hiss

Figures 3a–3f show the propagation characteristics of plasmaspheric hiss for Van Allen Probes from 19:00 UT to 21:00 UT. We adopt the techniques proposed by Santolík et al. (2002) and Santolík et al. (2003, 2010) to calculate the wave normal angles and Poynting fluxes from the wave spectral matrices measured by WFR of the EMFISIS suite. In the plasmaspheric plume (for Van Allen Probe A during 19:00–21:00 UT and for Van Allen Probe B during 19:00–19:25 UT), the hiss waves may be divided into two parts separated by 0.1 f_{ce} (f_{ce} is local electron gyrofrequency). The waves above 0.1 f_{ce} propagated away from the equator and had the ordered normal angles extending to $\psi = 50°$, indicating their near-equatorial generation by energetic electrons (He et al., 2019; Laakso et al., 2015). In contrast, the waves below 0.1 f_{ce} have disordered Poynting fluxes and normal angles, which

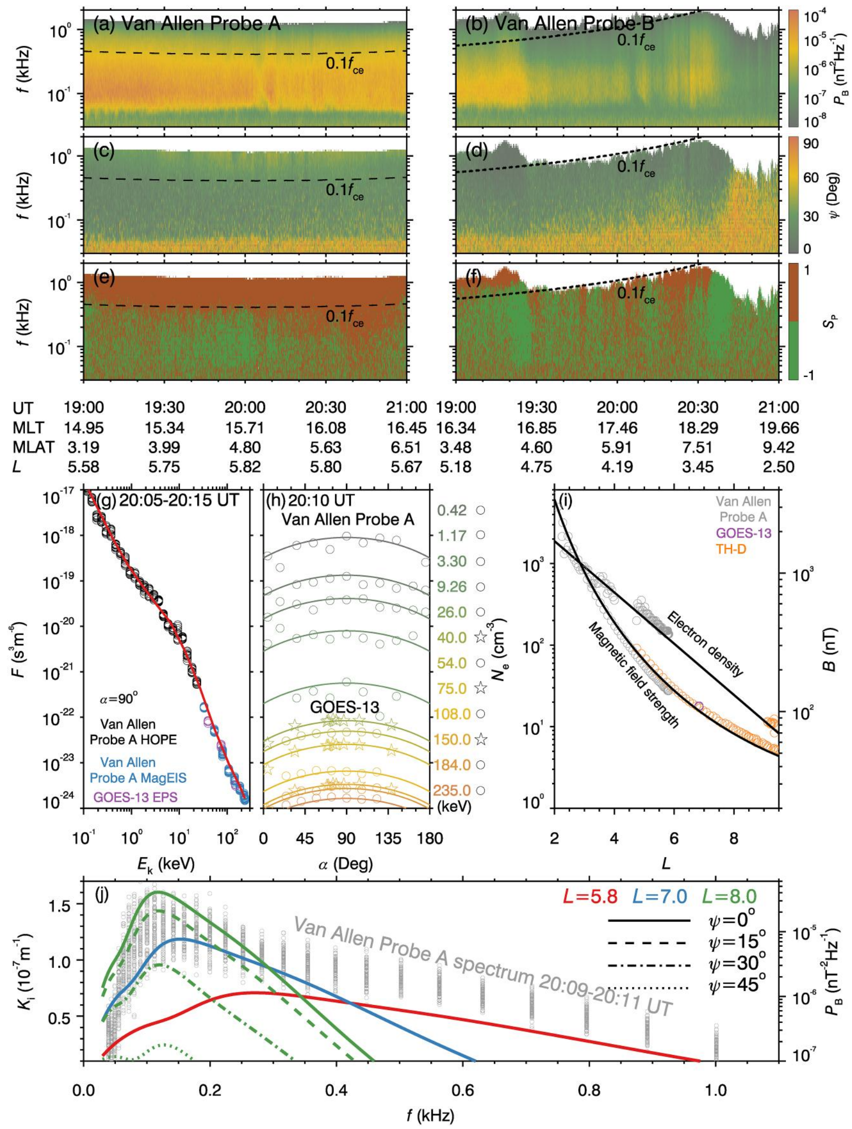

Figure 3. Identification for plasmaspheric hiss source. (a) and (b) Wave power spectral densities P_B, (c) and (d) normal angles ψ, and (e) and (f) Poynting flux directions S_p for Van Allen Probes A (left) and B (right), overlain by 0.1 f_{ce} (dashed lines). Note S_p represents the sign of wave Poynting flux component along the magnetic field line. (g) Observed (circles) and modeled (red line) electron phase space densities $F(\alpha = 90°)$ at the pitch-angle $\alpha = 90°$. Data are provided by HOPE (black) and MagEIS (blue) onboard Van Allen Probe A and EPS (purple) onboard GOES-13 during 20:05–20:15 UT. (h) Observed (symbols) and modeled (solid lines) electron pitch-angle distributions F. Colors help differentiate among the energy channels and symbols help differentiate between Van Allen Probe A (circles) and GOES-13 (stars). (i) Observed (circles) and modeled (black line) magnetic field strengths B and electron densities N_e. Data are from Van Allen Probe A (gray), GOES-13 (purple), and TH-D (orange) in the dayside orbits. (j) Linear growth rates of waves K_i at different L-shells (color-coded) and normal angles (indicated), in comparison to wave magnetic power spectral densities P_B measured by Van Allen Probe A around 20:10 UT.

should originate from some distant sources. Similarly, the irregularly-behaving hiss waves in the plasmaspheric core (for Van Allen Probe B during 19:25–21:00 UT) must have some distant sources. Lighting-generated whistler waves usually emerge at frequencies from hundreds of Hz to tens of kHz (Meredith et al., 2006; Santolík et al., 2021; Sonwalkar & Inan, 1989). As observed by TH-D (Figure 1g), the event-specific whistler-mode chorus waves occurred above 300 Hz outside the plasmasphere. We therefore speculate that the observed low-frequency hiss waves were generated in the duskside plasmaspheric plume (Laakso et al., 2015; Liu et al., 2020; Shi et al., 2019; Su et al., 2018a) far away from Earth (Figure 1b).

To examine the speculation above, we calculate the L-dependent linear growth rate of whistler-mode waves in the plasmaspheric plume at the equator, which is commonly considered a source region of hiss waves (Laakso et al., 2015; Su et al., 2018a; Wu et al., 2022). The specific code (Liu et al., 2018a, 2018b; Su et al., 2018a) is based on the linear instability theory (Chen et al., 2010; Kennel, 1966) and requires the inputs of electron phase space density F, cold electron density N_e and magnetic field strength B. Hiss waves are typically excited by electrons with energies above tens of keV (Chen et al., 2014; Su et al., 2018b; Thorne et al., 1973). These energetic electron phase space densities statistically vary little from $L = 5$ to $L = 8$ on the duskside (Li et al., 2010), as supported by present observations (Figures 3g and 3h) from the Helium Oxygen Proton and Electron (HOPE) mass spectrometer (Funsten et al., 2013) and the Magnetic Electron Ion Spectrometer (MagEIS) instrument (Blake et al., 2013) of the Energetic particle, Composition and the Thermal plasma (ECT) suite (Spence et al., 2013) onboard Van Allen Probe A ($L = 5.8$, MLAT = 5.1°, MLT = 15.8) and from the Energetic Particle Sensor (EPS) onboard GOES-13 ($L = 6.8$, MLAT = 9.4°, MLT = 15.3). Therefore, we assume a constant electron phase space distribution within $L = 5.8$–8. To remove random fluctuations, we average the phase space density in a 2-min window and model the pitch-angle dependence as $F = F(\alpha = 90°)\left(\frac{1+\sin\alpha}{2}\right)^2$. The radial density profile observed by Van Allen Probe A and TH-D in the plasmaspheric core and plume (Figure 3i) is well described by a previously-developed model (Carpenter & Anderson, 1992)

$$N_e = 10^{-0.3145L+3.9043}. \tag{2}$$

The magnetic fields observed by Van Allen Probe A, GOES-13 and TH-D (Figure 3i) at the magnetic latitudes MLAT < 10° during 16:00–23:30 UT are well described by a compressed dipole field model (Kabin et al., 2007) at the equator. In the spherical coordinate system (r, θ, ϕ), this magnetic field model is expressed as

$$\mathbf{B} = -\mathbf{e}_r\left[2B_0\left(\frac{R_E}{r}\right)^3 - B_{ex}\right]\cos\theta - \mathbf{e}_\theta\left[B_0\left(\frac{R_E}{r}\right)^3 + B_{ex}\right]\sin\theta \tag{3}$$

with $B_0 = 27{,}500$ nT and $B_{ex} = 16$ nT. Clearly, the linear growth rates peak at lower frequencies at larger magnetic shells (Figure 3j). The peak frequency of linear growth rates within $L = 7$–8 generally agrees with that of hiss wave power recorded by Van Allen Probe A in the near-base piece of the plasmaspheric plume. The increase of wave normal angles does not change the peak frequency of growth rates but reduces their peak value. As the normal angle ψ increases from 0° to 45°, the peak linear growth rate decreases by 85%. These modeling results suggest that the low-frequency (∼100 Hz) hiss waves were primarily generated at the quasi-parallel normal angles in the middle piece of the plasmaspheric plume ($L = 7$–8). Given the limited linear growth rate ($\sim 10^{-7}$ m^{-1}), additional nonlinear amplification may be required (Nakamura et al., 2016; Omura et al., 2015; Su et al., 2018a). Both Van Allen Probes A and B were located at the mid-way stations of hiss rays, and a more comprehensive evaluation of hiss lifetime has been left to the ray-tracing simulations.

4. Propagation of Plasmaspheric Hiss

We use the ray-tracing code of Kimura (1966) to understand the propagation of 90 Hz hiss waves from the middle piece of the plasmaspheric plume through the near-base piece to the plasmaspheric core. The background magnetic field is modeled by Equation 3. The corresponding background density is modeled with the same techniques of Wu et al. (2022) and Denton et al. (2002). To avoid duplication and facilitate readers, we here just give some general descriptions of the density model and list more details in the Supporting Information (Text S1 and Figures S1 and S2 in Supporting Information S1). As shown in Figure 4a, we analytically set the plasmaspheric core and plume boundaries and specify the background density base N_0 with Equation 2. To qualitatively describe the lumpy nature of the plasmaspheric plume (Borovsky & Denton, 2008; Nishimura et al., 2022), we additionally introduce the density ducts with the equatorial cross-section of $\Delta L = 0.05$ and ΔMLT = 0.01 hr (Figure 4b)

$$\delta N_e = N_0\left(\overline{N_{fl}} - 1\right), \tag{4}$$

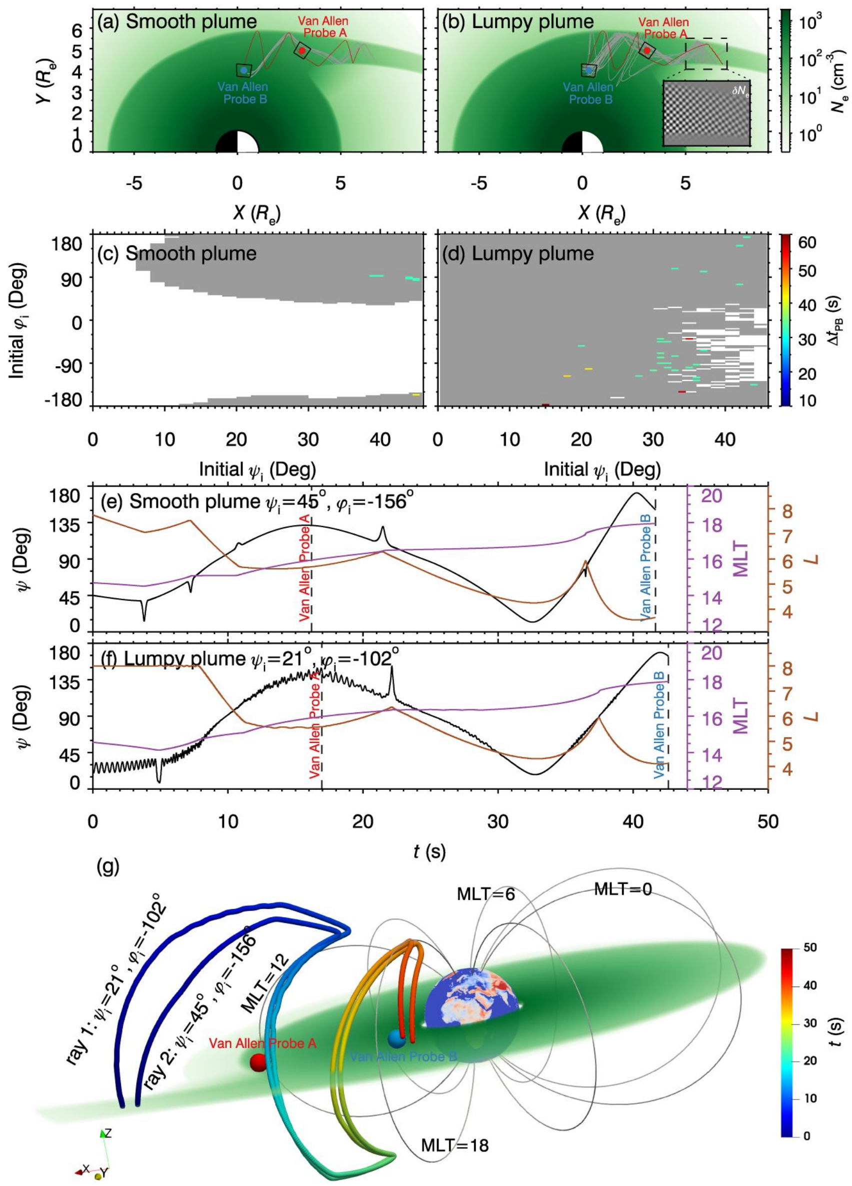

Figure 4. Ray-tracing modeling for $f = 90$ Hz hiss waves. Equatorial cross-section of the plasmasphere with (a) a smooth plume and (b) a lumpy plume. The electron density N_e is scaled by green saturation, and the gray and red lines are the projected paths of rays that are able to reach sufficiently close to Van Allen Probes A and B at 20:10 UT. The subpanel in Figure 4b plots the checkerboard density fluctuations δN_e scaled by the magnitude of black saturation. (c) and (d) Initial normal angles ψ_i and azimuthal angles φ_i of rays capable of migrating from source to plasmaspheric core (gray bins). Those rays that successively propagate through Van Allen Probes A and B are color-coded according to the propagation time from the plume source to Van Allen Probe B Δt_{PB}. (e) and (f) Wave normal angle ψ (black), magnetic shell L (brown), and magnetic local time MLT (purple) of selected rays (red lines) in Figures 4a and 4b. (g) Three-dimensional paths of selected rays (color-coded according to the propagation time). Van Allen Probes A and B at 20:10 UT are represented by red and blue solid spheres. The gray lines are the modeled geomagnetic field lines. The equatorial electron density is scaled by green saturation.

where the density fluctuation factor $\overline{N_{fl}}(L,\ \mathrm{MLT}) \in [0.9, 1.1]$. The transverse scale of density ducts is approximately 10–30 times the whistler wavelengths of our interest and the WKB approximation remains valid because the WKB parameter R_{WKB} (Horne & Thorne, 1997) is always below 0.1 in our following simulations.

According to the calculations in Figure 3, we launch the hiss rays of $f = 90$ Hz with normal angles $\psi_i \in [0°, 45°]$ spaced by 1° and azimuthal angles $\varphi_i \in (-180°, 180°]$ spaced by 3° at the equator of the middle piece $L \in [7, 8]$ of the plasmaspheric plume. Note that $\varphi = 0°$, 90°, and −90° correspond to the anti-earthward, eastward, and westward directions, respectively. Without density ducts, only the hiss rays with initial normal angles $\psi_i > 6°$ and azimuthal angles $|\varphi_i - 115°| < 85°$ can migrate into the plasmaspheric core (Figure 4c). The addition of density ducts allows almost all the hiss rays to migrate to the plasmaspheric core (Figure 4d). Because the plume hiss waves are generated primarily at the quasi-parallel normal angles, the ducting process appears to be crucial for the plume hiss waves to permeate the entire plasmasphere.

We select hiss rays that are able to reach sufficiently close to Van Allen Probes A and B at 20:10 UT: magnetic shell $|\Delta L| < 0.3$, magnetic local time $|\Delta \mathrm{MLT}| < 20$ min, and magnetic latitude $|\Delta \mathrm{MLAT}| < 3°$ (Figures 4a and 4b). These rays are scattered around the initial normal angles $\psi_i = 40°$ for the simulation with a smooth plume. In contrast, for the simulation with a lumpy plume, the initial normal angles of selected hiss rays have extended down to $\psi_i = 15°$. The total lifetimes of modeled hiss rays from the source region through Probe A to Probe B range from 33 to 69 s. These rays take 15–42 s from Probe A to Probe B, which, at least to some extent, explains the dispersion of the cross-correlation coefficient over the lag time (Figure 2f). We further elaborate two representative rays for the smooth ($\psi_i = 45°$, $\varphi_i = -156°$) and lumpy ($\psi_i = 21°$, $\varphi_i = -102°$) plumes (Figures 4a, 4b and 4e–4e), which take nearly the same time (25–26 s) from Probe A to Probe B (Figures 4e and 4f) as the "optimal" lag time derived from measurements (Figure 2f). The two rays exhibit the most significant difference in the normal angle. The addition of density ducts causes the repeated reflections of rays and then the fluctuations of normal angles. The total time of these hiss rays propagating from the plasmaspheric plume to the plasmaspheric core is 42 s, which may be interpreted as a lower limit of the hiss ray lifetime because of the absence of ray observations after passing through Van Allen Probe B.

5. Conclusion and Discussion

We set out to test the hypothesis that hiss waves have a long lifetime allowing themselves to permeate the global plasmasphere from a spatially restricted source. Although several modeling studies (Bortnik et al., 2003, 2008, 2011; Chen et al., 2009) predicted the lifetime of hiss rays on the order of 100 s, the propagation of hiss rays only within 2–6 s has been experimentally verified (Bortnik et al., 2009; Wang et al., 2011; Li et al., 2015; Wu et al., 2022). Our present observations and modeling establish the lower limit of 42 s for the lifetime of low-frequency hiss rays in the disturbed plasmasphere. These hiss waves were excited primarily along the field-aligned direction by energetic electrons near the equator in the middle piece (L = 7–8, MLT = 15) of the plasmaspheric plume. The modeled hiss rays can propagate from the middle piece (L = 7–8, MLT = 15) of the plasmaspheric plume, bounce between two hemispheres, pass through the near-base piece (L = 5.8, MLT = 15.8) of the plasmaspheric plume, and eventually drift into the plasmaspheric core (L = 4.1, MLT = 17.7). This mid-course propagation from the near-base piece of the plasmaspheric plume to the plasmaspheric core was fortunately detected by two magnetospheric spacecraft, whose elapsed time (∼27 s) is determined from the lag-correlation analysis of waves at the two places.

The migration of hiss waves from the plasmaspheric plume to the plasmaspheric core could largely benefit from the ducting process by the plasmaspheric density irregularities. Without these plasmaspheric density ducts, the quasi-parallel plume hiss waves would be difficult to enter the plasmaspheric core. In the low-altitude ionosphere, the gradient drift instability (Gondarenko & Guzdar, 2004; Keskinen et al., 2004; Rathod et al., 2021) and temperature gradient instability (Greenwald et al., 2006; Hudson & Kelley, 1976) can produce density fluctuations on a scale from several to tens of km, which may further cascade into fluctuations of 10 m scale (Eltrass et al., 2016; Heine et al., 2017; Nishimura et al., 2021). When mapped from the ionosphere to the magnetosphere, these density fluctuations appear as the field-aligned density ducts with cross-field sizes of ∼0.1–100 km (Gu et al., 2022; Nishimura et al., 2022). Other than the ionospheric instabilities, the local interchange instability and turbulent flow could also produce the small-scale density irregularities in the plasmaspheric plume (Borovsky & Denton, 2008; Huang et al., 1990; Rodger et al., 1998; Sazykin et al., 2002). These physical processes of small scales could eventually affect the large-scale distribution of plasmaspheric hiss waves.

Data Availability Statement

Van Allen Probes data are available at NASA's Space Physics Data Facility (SPDF) Website (2023); THEMIS data are available at THEMIS mission GOES mission homepage (2023); GOES data are available at GOES mission SPEDAS homepage (2023); ERG (Arase) data are available at ERG Science Center (2023) operated by ISAS/JAXA and ISEE/Nagoya University (Miyoshi, Hori, et al., 2018); SYM-H and AE data are available at World Data Center (WDC) for Geomagnetism Website (2023). In this work, we have analyzed the following data: (a) Van Allen Probes: EMFISIS L2 WFR Cross Spectral Matric data (Kletzing & Smith, 2022), L3 MAG magnetic field data (Kletzing, 2022b), L4 HFR density data (Kletzing, 2022a); EFW L2 1-second sensor potential data (Wygant, 2022); ECT L3 Release4 HOPE electron fluxes data (Funsten, 2022), MagEIS electron fluxes data (Spence et al., 2022); (b) THEMIS: FGM L2 magnetic field data (2023); ESA L2 spacecraft potential data (Angelopoulos, Carlson, & McFadden, 2023); SCM FFT power spectra of magnetic field data (Angelopoulos, Bonnell, et al., 2023); (c) Arase: MGF-L2 8s v03.02 data (Matsuoka, Teramoto, Imajo, et al., 2018); PWE/OFA-L3 spec v01_03 data (Kasahara, Kojima, et al., 2021); PWE/HFA-L3 v02_03 data (Kasahara, Kumamoto, et al., 2021); PWE/EFD-L2 potential v01_01 data (Kasahara et al., 2020); ORB-L2 v03 data (Miyoshi, Shinohara, & Jun 2018); (d) GOES-13: GOES 13 EPS/MAGD electron flux data (2023); GOES 13 MAG L2 magnetic field data (2023). Ray tracing program for Investigation of WAves Near the Earth (IWANE) is available at homepage of the Space Group of Kyoto University (Kimura, 2023). SPEDAS v5.0 code (Angelopoulos et al., 2019) for the electron density evaluation of THEMIS is downloaded from SPEDAS homepage (2023).

Acknowledgments

We acknowledge EMFISIS, EFW, and ECT teams for the use of Van Allen Probes data; FGM, ESA, and SCM teams for the use of THEMIS data; MGF and PWE teams for the use of Arase data; MAG and EPS teams for the use of GOES data and WDC for Geomagnetism (Kyoto) for the use of the SYM-H and AE indices. This work was supported by the Strategic Priority Research Program of Chinese Academy of Sciences grant XDB 41000000, the National Natural Science Foundation of China grants 42130204, 42188101, and 42274198, and the Key Research Program of the Chinese Academy of Sciences grant ZDRE-KT-2021-3.

References

Abel, B., & Thorne, R. M. (1998). Electron scattering loss in Earth's inner magnetosphere 1. Dominant physical processes. *Journal of Geophysical Research*, *103*(A2), 2385–2396. https://doi.org/10.1029/97JA02919

Angelopoulos, V. (2008). The THEMIS mission. *Space Science Reviews*, *141*(1–4), 5–34. https://doi.org/10.1007/s11214-008-9336-1

Angelopoulos, V., Bonnell, J. W., Cully, C. M., Roux, A., & Ergun, R. E. (2023). THEMIS-D: On Board Fast Fourier Transform (FFT) power spectra of Electric (EFI) and Magnetic (SCM) field measurements, for particle and wave burst survey modes [Dataset]. NASA Space Physics Data Facility. https://doi.org/10.48322/jj19-0q58

Angelopoulos, V., Carlson, C. W., & McFadden, J. P. (2023). THEMIS-D: ESA electron/ion energy fluxes and moments [Dataset]. NASA Space Physics Data Facility. https://doi.org/10.48322/05m2-0k28

Angelopoulos, V., Cruce, P., Drozdov, A., Grimes, E. W., Hatzigeorgiu, N., King, D. A., et al. (2019). The Space Physics Environment Data Analysis System (SPEDAS). *Space Science Reviews*, *215*(1), 9. https://doi.org/10.1007/s11214-018-0576-4

Auster, H. U., Glassmeier, K. H., Magnes, W., Aydogar, O., Baumjohann, W., Constantinescu, D., et al. (2008). The THEMIS Fluxgate Magnetometer. *Space Science Reviews*, *141*(1–4), 235–264. https://doi.org/10.1007/s11214-008-9365-9

Blake, J. B., Carranza, P. A., Claudepierre, S. G., Clemmons, J. H., Crain, W. R., Dotan, Y., et al. (2013). The magnetic electron ion spectrometer (MagEIS) instruments aboard the radiation belt storm probes (RBSP) spacecraft. *Space Science Reviews*, *179*(1–4), 383–421. https://doi.org/10.1007/s11214-013-9991-8

Borovsky, J. E., & Denton, M. H. (2008). A statistical look at plasmaspheric drainage plumes. *Journal of Geophysical Research*, *113*(A9), A09221. https://doi.org/10.1029/2007JA012994

Bortnik, J., Chen, L., Li, W., Thorne, R. M., & Horne, R. B. (2011). Modeling the evolution of chorus waves into plasmaspheric hiss. *Journal of Geophysical Research*, *116*(A8), 8221. https://doi.org/10.1029/2011JA016499

Bortnik, J., Inan, U. S., & Bell, T. F. (2003). Energy distribution and lifetime of magnetospherically reflecting whistlers in the plasmasphere. *Journal of Geophysical Research*, *108*(A5), 1199. https://doi.org/10.1029/2002JA009316

Bortnik, J., Li, W., Thorne, R. M., Angelopoulos, V., Cully, C., Bonnell, J., et al. (2009). An observation linking the origin of plasmaspheric hiss to discrete chorus emissions. *Science*, *324*(5928), 775–778. https://doi.org/10.1126/science.1171273

Bortnik, J., Thorne, R. M., & Meredith, N. P. (2008). The unexpected origin of plasmaspheric hiss from discrete chorus emissions. *Nature*, *452*(7183), 62–66. https://doi.org/10.1038/nature06741

Breneman, A. W., Halford, A., Millan, R., McCarthy, M., Fennell, J., Sample, J., et al. (2015). Global-scale coherence modulation of radiation-belt electron loss from plasmaspheric hiss. *Nature*, *523*(7559), 193–195. https://doi.org/10.1038/nature14515

Carpenter, D. L., & Anderson, R. R. (1992). An ISEE/whistler model of equatorial electron density in the magnetosphere. *Journal of Geophysical Research*, *97*(A2), 1097–1108. https://doi.org/10.1029/91ja01548

Chan, K., & Holzer, R. E. (1976). ELF hiss associated with plasma density enhancements in the outer magnetosphere. *Journal of Geophysical Research*, *81*(13), 2267–2274. https://doi.org/10.1029/JA081i013p02267

Chen, L., Bortnik, J., Thorne, R. M., Horne, R. B., & Jordanova, V. K. (2009). Three-dimensional ray tracing of VLF waves in a magnetospheric environment containing a plasmaspheric plume. *Geophysical Research Letters*, *36*(22), 22101. https://doi.org/10.1029/2009GL040451

Chen, L., Pfaff, R., Heelis, R., Boardsen, S., & Xia, Z. (2020). Ion cyclotron resonant absorption lines in ELF hiss power spectral density in the low-latitude ionosphere. *Geophysical Research Letters*, *47*(2), e86315. https://doi.org/10.1029/2019GL086315

Chen, L., Thorne, R. M., Bortnik, J., Li, W., Horne, R. B., Reeves, G. D., et al. (2014). Generation of unusually low frequency plasmaspheric hiss. *Geophysical Research Letters*, *41*(16), 5702–5709. https://doi.org/10.1002/2014GL060628

Chen, L., Thorne, R. M., Jordanova, V. K., Wang, C.-P., Gkioulidou, M., Lyons, L., & Horne, R. B. (2010). Global simulation of EMIC wave excitation during the 21 April 2001 storm from coupled RCM-RAM-HOTRAY modeling. *Journal of Geophysical Research*, *115*(A7), 7209. https://doi.org/10.1029/2009JA015075

Davis, G. K. (2007). History of the NOAA satellite program. *Journal of Applied Remote Sensing*, *1*(1), 012504. https://doi.org/10.1117/1.2642347

Denton, R. E., Goldstein, J., & Menietti, J. D. (2002). Field line dependence of magnetospheric electron density. *Geophysical Research Letters*, *29*(24), 2205. https://doi.org/10.1029/2002GL015963

Dunckel, N., & Helliwell, R. A. (1969). Whistler-mode emissions on the OGO 1 satellite. *Journal of Geophysical Research*, *74*(26), 6371–6385. https://doi.org/10.1029/JA074i026p06371

Eltrass, A., Scales, W. A., Erickson, P. J., Ruohoniemi, J. M., & Baker, J. B. H. (2016). Investigation of the role of plasma wave cascading processes in the formation of midlatitude irregularities utilizing GPS and radar observations. *Radio Science*, *51*(6), 836–851. https://doi.org/10.1002/2015RS005790

ERG Science Center. (2023). The ERG Science Center. Retrieved from https://ergsc.isee.nagoya-u.ac.jp/index.shtml.en

FGM L2 magnetic field data. (2023). The Fluxgate Magnetometer (FGM) Level 2 data. [Dataset]. Retrieved from https://spdf.gsfc.nasa.gov/pub/data/themis/thd/l2/fgm/

Fu, S., Yi, J., Ni, B., Zhou, R., Hu, Z., Cao, X., et al. (2020). Combined scattering of radiation belt electrons by low-frequency hiss: Cyclotron, c, and bounce resonances. *Geophysical Research Letters*, *47*(5), e86963. https://doi.org/10.1029/2020GL086963

Funsten, H. O. (2022). Van Allen Probe A Energetic Particle, Composition, and Thermal Plasma Suite (ECT) Helium oxygen Proton electron, HOPE, mass spectrometer pitch angle resolved science data. Electron fluxes, 15 eV to 50 keV, and ion fluxes, 1 eV to 50 keV, as measured in alternate Spin Cadence, Level 3, Release 4 (L3), 11.35 s data. [Dataset]. NASA Space Physics Data Facility. https://doi.org/10.48322/17p9-rf75

Funsten, H. O., Skoug, R. M., Guthrie, A. A., MacDonald, E. A., Baldonado, J. R., Harper, R. W., et al. (2013). Helium, Oxygen, Proton, and Electron (HOPE) mass spectrometer for the radiation belt storm probes mission. *Space Science Reviews*, *179*(1–4), 423–484. https://doi.org/10.1007/s11214-013-9968-7

Gallagher, D. L., Adrian, M. L., & Liemohn, M. W. (2005). Origin and evolution of deep plasmaspheric notches. *Journal of Geophysical Research*, *110*(A9), A09201. https://doi.org/10.1029/2004JA010906

GOES 13 EPS/MAGD electron flux data. (2023). GOES 13 Magnetospheric Electron Detector (MAGED) electron flux data. [Dataset]. Retrieved from https://spdf.gsfc.nasa.gov/pub/data/goes/goes13/

GOES 13 MAG L2 magnetic field data. (2023). GOES 13 fluxgate magnetometer (MAG) data. [Dataset]. Retrieved from https://spdf.gsfc.nasa.gov/pub/data/goes/goes13/

GOES mission homepage. (2023). Geostationary Operational Environmental Satellites (GOES) data. [Dataset]. Retrieved from https://www.ngdc.noaa.gov/stp/satellite/goes/index.html

Gondarenko, N. A., & Guzdar, P. N. (2004). Density and electric field fluctuations associated with the gradient drift instability in the high-latitude ionosphere. *Geophysical Research Letters*, *31*(11), L11802. https://doi.org/10.1029/2004GL019703

Green, A., Li, W., Ma, Q., Shen, X. C., Bortnik, J., & Hospodarsky, G. B. (2020). Properties of lightning generated whistlers based on Van Allen Probes observations and their global effects on radiation belt electron loss. *Geophysical Research Letters*, *47*(17), e89584. https://doi.org/10.1029/2020GL089584

Greenwald, R. A., Oksavik, K., Erickson, P. J., Lind, F. D., Ruohoniemi, J. M., Baker, J. B. H., & Gjerloev, J. W. (2006). Identification of the temperature gradient instability as the source of decameter-scale ionospheric irregularities on plasmapause field lines. *Geophysical Research Letters*, *33*(18), L18105. https://doi.org/10.1029/2006GL026581

Gu, W., Liu, X., Xia, Z., & Chen, L. (2022). Statistical study on small-scale (≤1,000 km) density irregularities in the inner magnetosphere. *Journal of Geophysical Research: Space Physics*, *127*(7), e30574. https://doi.org/10.1029/2022JA030574

He, Z., Chen, L., Liu, X., Zhu, H., Liu, S., Gao, Z., & Cao, Y. (2019). Local generation of high-frequency plasmaspheric hiss observed by Van Allen Probes. *Geophysical Research Letters*, *46*(3), 1141–1148. https://doi.org/10.1029/2018GL081578

Heine, T. R. P., Moldwin, M. B., & Zou, S. (2017). Small-scale structure of the midlatitude storm enhanced density plume during the 17 March 2015 St. Patrick's Day storm. *Journal of Geophysical Research (Space Physics)*, *122*(3), 3665–3677. https://doi.org/10.1002/2016JA022965

Horne, R. B., & Thorne, R. M. (1997). Wave heating of He^+ by electromagnetic ion cyclotron waves in the magnetosphere: Heating near the H^+-He^+ bi-ion resonance frequency. *Journal of Geophysical Research*, *102*(A6), 11457–11472. https://doi.org/10.1029/97JA00749

Huang, T. S., Wolf, R. A., & Hill, T. W. (1990). Interchange instability of the Earth's plasmapause. *Journal of Geophysical Research*, *95*(A10), 17187–17198. https://doi.org/10.1029/JA095iA10p17187

Hudson, M. K., & Kelley, M. C. (1976). The temperature gradient drift instability at the equatorward edge of the ionospheric plasma trough. *Journal of Geophysical Research*, *81*(22), 3913–3918. https://doi.org/10.1029/JA081i022p03913

Kabin, K., Rankin, R., Mann, I. R., Degeling, A. W., & Marchand, R. (2007). Polarization properties of standing shear Alfvén waves in non-axisymmetric background magnetic fields. *Annales Geophysicae*, *25*(3), 815–822. https://doi.org/10.5194/angeo-25-815-2007

Kasaba, Y., Ishisaka, K., Kasahara, Y., Imachi, T., Yagitani, S., Kojima, H., et al. (2017). Wire Probe Antenna (WPT) and Electric Field Detector (EFD) of Plasma Wave Experiment (PWE) aboard the Arase satellite: Specifications and initial evaluation results. *Earth Planets and Space*, *69*(1), 174. https://doi.org/10.1186/s40623-017-0760-x

Kasahara, Y., Kasaba, Y., Kojima, H., Yagitani, S., Ishisaka, K., Kumamoto, A., et al. (2018). The Plasma Wave Experiment (PWE) on board the Arase (ERG) satellite. *Earth Planets and Space*, *70*(1), 86. https://doi.org/10.1186/s40623-018-0842-4

Kasahara, Y., Kasaba, Y., Matsuda, S., Shoji, M., Nakagawa, T., Ishisaka, K., et al. (2020). The PWE/EFD instrument Level-2 potential waveform data of Exploration of energization and Radiation in Geospace (ERG) Arase satellite. [Dataset]. ERG. https://doi.org/10.34515/DATA.ERG-07002

Kasahara, Y., Kojima, H., Matsuda, S., Ozaki, M., Yagitani, S., Matsuoka, A., et al. (2021). The PWE/OFA instrument Level-3 wave property data of Exploration of energization and Radiation in Geospace (ERG) Arase satellite. [Dataset]. ERG. https://doi.org/10.34515/DATA.ERG-08003

Kasahara, Y., Kumamoto, A., Tsuchiya, F., Kojima, H., Matsuda, S., Matsuoka, A., et al. (2021). The PWE/HFA instrument Level-3 electron density data of Exploration of energization and Radiation in Geospace (ERG) Arase satellite. [Dataset]. ERG. https://doi.org/10.34515/DATA.ERG-10001

Kazama, Y., Kojima, H., Miyoshi, Y., Kasahara, Y., Usui, H., Wang, B. J., et al. (2018). Density depletions associated with enhancements of electron cyclotron harmonic emissions: An ERG observation. *Geophysical Research Letters*, *45*(19), 10075–10083. https://doi.org/10.1029/2018GL080117

Kennel, C. (1966). Low-frequency whistler mode. *Physics of Fluids*, *9*(11), 2190–2202. https://doi.org/10.1063/1.1761588

Keskinen, M. J., Basu, S., & Basu, S. (2004). Midlatitude sub-auroral ionospheric small scale structure during a magnetic storm. *Geophysical Research Letters*, *31*(9), L09811. https://doi.org/10.1029/2003GL019368

Kimura, I. (1966). Effects of ions on whistler-mode ray tracing. *Radio Science*, *1*(3), 269–284. https://doi.org/10.1002/rds196613269

Kimura, I. (2023). Ray tracing program for investigation of WAves Near the Earth (IWANE). [Software]. Retrieved from http://space.rish.kyoto-u.ac.jp/software/

Kintner, P. M., Scales, W., Vago, J., Yau, A., Whalen, B., Arnoldy, R., & Moore, T. (1991). Harmonic H^+ gyrofrequency structures in auroral hiss observed by high-altitude auroral sounding rockets. *Journal of Geophysical Research*, *96*(A6), 9627–9638. https://doi.org/10.1029/91JA00563

Kletzing, C. A. (2022a). Van Allen Probe A Electric and Magnetic Field Instrument Suite and Integrated Science (EMFISIS) density and other parameters derived by digitizing traces on spectrograms, Level 4 (L4), 0.5 s data. [Dataset]. NASA Space Physics Data Facility. https://doi.org/10.48322/c4ha-xj50

Kletzing, C. A. (2022b). Van Allen Probe A Fluxgate Magnetometer 1 second resolution data in GSM coordinates. [Dataset]. NASA Space Physics Data Facility. https://doi.org/10.48322/w6r4-fp76

Kletzing, C. A., Kurth, W. S., Acuna, M., MacDowall, R. J., Torbert, R. B., Averkamp, T., et al. (2013). The Electric and Magnetic Field Instrument Suite and Integrated Science (EMFISIS) on RBSP. *Space Science Reviews*, *179*(1–4), 127–181. https://doi.org/10.1007/s11214-013-9993-6

Kletzing, C. A., & Smith, C. W. (2022). Van Allen Probe A Electric and Magnetic Field Instrument Suite and Integrated Science (EMFISIS) Waveform Receiver (WFR) cross spectral Matrix, Level 2 (L2), 6 s data. [Dataset]. NASA Space Physics Data Facility. https://doi.org/10.48322/be1v-n754

Kumamoto, A., Tsuchiya, F., Kasahara, Y., Kasaba, Y., Kojima, H., Yagitani, S., et al. (2018). High Frequency Analyzer (HFA) of Plasma Wave Experiment (PWE) onboard the Arase spacecraft. *Earth Planets and Space*, *70*(1), 82. https://doi.org/10.1186/s40623-018-0854-0

Kurth, W. S., De Pascuale, S., Faden, J. B., Kletzing, C. A., Hospodarsky, G. B., Thaller, S., & Wygant, J. R. (2015). Electron densities inferred from plasma wave spectra obtained by the Waves instrument on Van Allen Probes. *Journal of Geophysical Research: Space Physics*, *120*(2), 904–914. https://doi.org/10.1002/2014JA020857

Laakso, H., Santolik, O., Horne, R., Kolmasová, I., Escoubet, P., Masson, A., & Taylor, M. (2015). Identifying the source region of plasmaspheric hiss. *Geophysical Research Letters*, *42*(9), 3141–3149. https://doi.org/10.1002/2015GL063755

Li, J., Ma, Q., Bortnik, J., Li, W., An, X., Reeves, G. D., et al. (2019). Parallel acceleration of suprathermal electrons caused by whistler-mode hiss waves. *Geophysical Research Letters*, *46*(22), 12675–12684. https://doi.org/10.1029/2019GL085562

Li, W., Chen, L., Bortnik, J., Thorne, R. M., Angelopoulos, V., Kletzing, C. A., et al. (2015). First evidence for chorus at a large geocentric distance as a source of plasmaspheric hiss: Coordinated THEMIS and Van Allen Probes observation. *Geophysical Research Letters*, *42*(2), 241–248. https://doi.org/10.1002/2014GL062832

Li, W., Shprits, Y. Y., & Thorne, R. M. (2007). Dynamic evolution of energetic outer zone electrons due to wave-particle interactions during storms. *Journal of Geophysical Research*, *112*(A10), A10220. https://doi.org/10.1029/2007JA012368

Li, W., Thorne, R. M., Bortnik, J., Reeves, G. D., Kletzing, C. A., Kurth, W. S., et al. (2013). An unusual enhancement of low-frequency plasmaspheric hiss in the outer plasmasphere associated with substorm-injected electrons. *Geophysical Research Letters*, *40*(15), 3798–3803. https://doi.org/10.1002/grl.50787

Li, W., Thorne, R. M., Nishimura, Y., Bortnik, J., Angelopoulos, V., McFadden, J. P., et al. (2010). THEMIS analysis of observed equatorial electron distributions responsible for the chorus excitation. *Journal of Geophysical Research*, *115*(1), A00F11. https://doi.org/10.1029/2009JA014845

Liu, N., Su, Z., Gao, Z., Zheng, H., Wang, Y., Wang, S., et al. (2020). Comprehensive observations of substorm-enhanced plasmaspheric hiss generation, propagation, and dissipation. *Geophysical Research Letters*, *47*(2), e86040. https://doi.org/10.1029/2019GL086040

Liu, N., Su, Z., Zheng, H., Wang, Y., & Wang, S. (2018a). Magnetosonic harmonic falling and rising frequency emissions potentially generated by nonlinear wave-wave interactions in the Van Allen radiation belts. *Geophysical Research Letters*, *45*(16), 7985–7995. https://doi.org/10.1029/2018GL079232

Liu, N., Su, Z., Zheng, H., Wang, Y., & Wang, S. (2018b). Prompt disappearance and emergence of radiation belt magnetosonic waves induced by solar wind dynamic pressure variations. *Geophysical Research Letters*, *45*(2), 585–594. https://doi.org/10.1002/2017GL076382

Lyons, L. R., & Thorne, R. M. (1973). Equilibrium structure of radiation belt electrons. *Journal of Geophysical Research*, *78*(13), 2142–2149. https://doi.org/10.1029/JA078i013p02142

Lyons, L. R., Thorne, R. M., & Kennel, C. F. (1972). Pitch-angle diffusion of radiation belt electrons within the plasmasphere. *Journal of Geophysical Research*, *77*(19), 3455–3474. https://doi.org/10.1029/JA077i019p03455

Matsuda, S., Kasahara, Y., Kojima, H., Kasaba, Y., Yagitani, S., Ozaki, M., et al. (2018). Onboard software of plasma wave experiment aboard Arase: Instrument management and signal processing of waveform capture/onboard frequency analyzer. *Earth Planets and Space*, *70*(1), 75. https://doi.org/10.1186/s40623-018-0838-0

Matsuoka, A., Teramoto, M., Imajo, S., Kurita, S., Miyoshi, Y., & Shinohara, I. (2018). The MGF instrument Level-2 spin-averaged magnetic field data of Exploration of energization and Radiation in Geospace (ERG) Arase satellite. [Dataset]. ERG. https://doi.org/10.34515/DATA.ERG-06001

Matsuoka, A., Teramoto, M., Nomura, R., Nosé, M., Fujimoto, A., Tanaka, Y., et al. (2018). The ARASE (ERG) magnetic field investigation. *Earth Planets and Space*, *70*(1), 43. https://doi.org/10.1186/s40623-018-0800-1

Mauk, B. H., Fox, N. J., Kanekal, S. G., Kessel, R. L., Sibeck, D. G., & Ukhorskiy, A. (2013). Science objectives and rationale for the Radiation Belt Storm Probes mission. *Space Science Reviews*, *179*(1–4), 3–27. https://doi.org/10.1007/s11214-012-9908-y

McFadden, J. P., Carlson, C. W., Larson, D., Ludlam, M., Abiad, R., Elliott, B., et al. (2008). The THEMIS ESA plasma instrument and in-flight calibration. *Space Science Reviews*, *141*(1–4), 277–302. https://doi.org/10.1007/s11214-008-9440-2

Meredith, N. P., Horne, R. B., Bortnik, J., Thorne, R. M., Chen, L., Li, W., & Sicard-Piet, A. (2013). Global statistical evidence for chorus as the embryonic source of plasmaspheric hiss. *Geophysical Research Letters*, *40*(12), 2891–2896. https://doi.org/10.1002/grl.50593

Meredith, N. P., Horne, R. B., Clilverd, M. A., Horsfall, D., Thorne, R. M., & Anderson, R. R. (2006). Origins of plasmaspheric hiss. *Journal of Geophysical Research*, *111*(A10). 9217-+. https://doi.org/10.1029/2006JA011707

Meredith, N. P., Horne, R. B., Thorne, R. M., Summers, D., & Anderson, R. R. (2004). Substorm dependence of plasmaspheric hiss. *Journal of Geophysical Research*, *109*(A6), A06209. https://doi.org/10.1029/2004JA010387

Miyoshi, Y., Hori, T., Shoji, M., Teramoto, M., Chang, T. F., Segawa, T., et al. (2018). The ERG Science Center. *Earth Planets and Space*, *70*(1), 96. https://doi.org/10.1186/s40623-018-0867-8

Miyoshi, Y., Shinohara, I., & Jun, C. W. (2018). The Level-2 orbit data of Exploration of energization and Radiation in Geospace (ERG) Arase satellite. [Dataset]. ERG. https://doi.org/10.34515/DATA.ERG-12000

Miyoshi, Y., Shinohara, I., Takashima, T., Asamura, K., Higashio, N., Mitani, T., et al. (2018). Geospace exploration project ERG. *Earth Planets and Space*, *70*(1), 101. https://doi.org/10.1186/s40623-018-0862-0

Miyoshi, Y., Shinohara, I., Ukhorskiy, S., Claudepierre, S. G., Mitani, T., Takashima, T., et al. (2022). Collaborative Research activities of the Arase and Van Allen Probes. *Space Science Reviews*, *218*(5), 38. https://doi.org/10.1007/s11214-022-00885-4

Nakamura, S., Omura, Y., Summers, D., & Kletzing, C. A. (2016). Observational evidence of the nonlinear wave growth theory of plasmaspheric hiss. *Geophysical Research Letters*, *43*(19), 10. https://doi.org/10.1002/2016GL070333

NASA's Space Physics Data Facility (SPDF) Website. (2023). NASA's Space Physics Data Facility (SPDF). [Dataset]. Retrieved from https://spdf.gsfc.nasa.gov/pub/data/rbsp/

Ni, B., Bortnik, J., Thorne, R. M., Ma, Q., & Chen, L. (2013). Resonant scattering and resultant pitch angle evolution of relativistic electrons by plasmaspheric hiss. *Journal of Geophysical Research: Space Physics*, *118*(12), 7740–7751. https://doi.org/10.1002/2013JA019260

Ni, B., Huang, H., Zhang, W., Gu, X., Zhao, H., Li, X., et al. (2019). Parametric sensitivity of the formation of reversed electron energy spectrum caused by plasmaspheric hiss. *Geophysical Research Letters*, *46*(8), 4134–4143. https://doi.org/10.1029/2019GL082032

Ni, B., Summers, D., Xiang, Z., Dou, X., Tsurutani, B. T., Meredith, N. P., et al. (2023). Unique banded structures of plasmaspheric hiss waves in the Earth's magnetosphere. *Journal of Geophysical Research (Space Physics)*, *128*(3). e2023JA031325. https://doi.org/10.1029/2023JA031325

Nishimura, Y., Bortnik, J., Li, W., Thorne, R. M., Ni, B., Lyons, L. R., et al. (2013). Structures of dayside whistler-mode waves deduced from conjugate diffuse aurora. *Journal of Geophysical Research: Space Physics*, *118*(2), 664–673. https://doi.org/10.1029/2012JA018242

Nishimura, Y., Goldstein, J., Martinis, C., Ma, Q., Li, W., Zhang, S. R., et al. (2022). Multi-scale density structures in the plasmaspheric plume during a geomagnetic storm. *Journal of Geophysical Research: Space Physics*, *127*(3), e30230. https://doi.org/10.1029/2021JA030230

Nishimura, Y., Mrak, S., Semeter, J. L., Coster, A. J., Jayachandran, P. T., Groves, K. M., et al. (2021). Evolution of mid-latitude density irregularities and scintillation in North America during the 7-8 September 2017 storm. *Journal of Geophysical Research (Space Physics)*, *126*(6), e29192. https://doi.org/10.1029/2021JA029192

Omura, Y., Nakamura, S., Kletzing, C. A., Summers, D., & Hikishima, M. (2015). Nonlinear wave growth theory of coherent hiss emissions in the plasmasphere. *Journal of Geophysical Research*, *120*(9), 7642–7657. https://doi.org/10.1002/2015JA021520

Rathod, C., Srinivasan, B., Scales, W., & Kunduri, B. (2021). Investigation of the gradient drift instability as a cause of density irregularities in subauroral polarization streams. *Journal of Geophysical Research (Space Physics)*, *126*(5), e29027. https://doi.org/10.1029/2020JA029027

Rodger, C. J., Thomson, N. R., & Dowden, R. L. (1998). Are whistler ducts created by thunderstorm electrostatic fields? *Journal of Geophysical Research*, *103*(A2), 2163–2170. https://doi.org/10.1029/97JA02927

Roux, A., Le Contel, O., Coillot, C., Bouabdellah, A., de La Porte, B., Alison, D., et al. (2008). The Search coil magnetometer for THEMIS. *Space Science Reviews*, *141*(1–4), 265–275. https://doi.org/10.1007/s11214-008-9455-8

Russell, C. T., Holzer, R. E., & Smith, E. J. (1969). OGO 3 observations of ELF noise in the magnetosphere. 1. Spatial extent and frequency of occurrence. *Journal of Geophysical Research*, *74*, 755–777. https://doi.org/10.1029/JA074i003p00755

Santolík, O., Kolmašová, I., Pickett, J. S., & Gurnett, D. A. (2021). Multi-point observation of hiss emerging from lightning whistlers. *Journal of Geophysical Research: Space Physics*, *126*(12), e29524. https://doi.org/10.1029/2021JA029524

Santolík, O., Parrot, M., & Lefeuvre, F. (2003). Singular value decomposition methods for wave propagation analysis. *Radio Science*, *38*(1), 1010. https://doi.org/10.1029/2000RS002523

Santolík, O., Pickett, J. S., Gurnett, D. A., Menietti, J. D., Tsurutani, B. T., & Verkhoglyadova, O. (2010). Survey of Poynting flux of whistler mode chorus in the outer zone. *Journal of Geophysical Research*, *115*(A7), A00F13. https://doi.org/10.1029/2009JA014925

Santolík, O., Pickett, J. S., Gurnett, D. A., & Storey, L. R. O. (2002). Magnetic component of narrowband ion cyclotron waves in the auroral zone. *Journal of Geophysical Research*, *107*(A12), 1444. https://doi.org/10.1029/2001JA000146

Sazykin, S., Wolf, R. A., Spiro, R. W., Gombosi, T. I., De Zeeuw, D. L., & Thomsen, M. F. (2002). Interchange instability in the inner magnetosphere associated with geosynchronous particle flux decreases. *Geophysical Research Letters*, *29*(10), 1448. https://doi.org/10.1029/2001GL014416

Shi, R., Li, W., Ma, Q., Green, A., Kletzing, C. A., Kurth, W. S., et al. (2019). Properties of whistler mode waves in earth's plasmasphere and plumes. *Journal of Geophysical Research*, *124*(2), 1035–1051. https://doi.org/10.1029/2018JA026041

Shprits, Y. Y. (2009). Potential waves for pitch-angle scattering of near-equatorially mirroring energetic electrons due to the violation of the second adiabatic invariant. *Geophysical Research Letters*, *36*(12), L12106. https://doi.org/10.1029/2009GL038322

Sonwalkar, V. S., & Inan, U. S. (1989). Lightning as an embryonic source of VLF hiss. *Journal of Geophysical Research*, *94*, 6986–6994. https://doi.org/10.1029/JA094iA06p06986

SPEDAS homepage. (2023). Space Physics Environment Data Analysis Software (SPEDAS). [Software]. Retrieved from https://spedas.org/blog/

Spence, H. E., Reeves, G. D., Baker, D. N., Blake, J. B., Bolton, M., Bourdarie, S., et al. (2013). Science goals and overview of the Radiation Belt Storm Probes (RBSP) Energetic Particle, Composition, and Thermal Plasma (ECT) suite on NASA's Van Allen Probes mission. *Space Science Reviews*, *179*(1–4), 311–336. https://doi.org/10.1007/s11214-013-0007-5

Spence, H. E., Reeves, G. D., & Blake, J. B. (2022). Van Allen Probe A Energetic Particle, Composition, and Thermal Plasma Suite (ECT) Magnetic Electron Ion Spectrometer (MagEIS), Electron Fluxes, 20 to 4000 keV, Proton Fluxes, 60 to 1500 keV, Level 3, Release 4 (L3), 10.9 s data. [Dataset]. NASA Space Physics Data Facility. https://doi.org/10.48322/09qz-tf17

Su, Z., Liu, N., Zheng, H., Wang, Y., & Wang, S. (2018a). Large-amplitude extremely low frequency hiss waves in plasmaspheric plumes. *Geophysical Research Letters*, *45*(2), 565–577. https://doi.org/10.1002/2017GL076754

Su, Z., Liu, N., Zheng, H., Wang, Y., & Wang, S. (2018b). Multipoint observations of nightside plasmaspheric hiss generated by substorm-injected electrons. *Geophysical Research Letters*, *45*(20), 10. https://doi.org/10.1029/2018GL079927

Summers, D., Ni, B., Meredith, N. P., Horne, R. B., Thorne, R. M., Moldwin, M. B., & Anderson, R. R. (2008). Electron scattering by whistler-mode ELF hiss in plasmaspheric plumes. *Journal of Geophysical Research*, *113*(A4), A04219. https://doi.org/10.1029/2007JA012678

THEMIS mission homepage. (2023). Time History of Events and Macroscale Interactions during Substorms (THEMIS) data. [Dataset]. Retrieved from http://themis.ssl.berkeley.edu/data/themis/

Thorne, R. M., & Horne, R. B. (1994). Landau damping of magnetospherically reflected whistlers. *Journal of Geophysical Research*, *99*(A9), 17249–17258. https://doi.org/10.1029/94JA01006

Thorne, R. M., Li, W., Ni, B., Ma, Q., Bortnik, J., Baker, D. N., et al. (2013). Evolution and slow decay of an unusual narrow ring of relativistic electrons near L ˜3.2 following the September 2012 magnetic storm. *Geophysical Research Letters*, *40*(14), 3507–3511. https://doi.org/10.1002/grl.50627

Thorne, R. M., Smith, E. J., Burton, R. K., & Holzer, R. E. (1973). Plasmaspheric hiss. *Journal of Geophysical Research*, *78*(10), 1581–1596. https://doi.org/10.1029/JA078i010p01581

Tsurutani, B. T., Falkowski, B. J., Pickett, J. S., Santolik, O., & Lakhina, G. S. (2015). Plasmaspheric hiss properties: Observations from Polar. *Journal of Geophysical Research*, *120*(1), 414–431. https://doi.org/10.1002/2014JA020518

Wang, C., Zong, Q., Xiao, F., Su, Z., Wang, Y., & Yue, C. (2011). The relations between magnetospheric chorus and hiss inside and outside the plasmasphere boundary layer: Cluster observation. *Journal of Geophysical Research*, *116*(A7), A07221. https://doi.org/10.1029/2010JA016240

Wang, Z., Su, Z., Liu, N., Dai, G., Zheng, H., Wang, Y., & Wang, S. (2020). Suprathermal electron evolution under the competition between plasmaspheric plume hiss wave heating and collisional cooling. *Geophysical Research Letters*, *47*(19), e89649. https://doi.org/10.1029/2020GL089649

Woodroffe, J. R., & Streltsov, A. V. (2014). Whistler interaction with field-aligned density irregularities in the ionosphere: Refraction, diffraction, and interference. *Journal of Geophysical Research: Space Physics*, *119*(7), 5790–5799. https://doi.org/10.1002/2013JA019683

World Data Center (WDC) for Geomagnetism Website. (2023). World Data Center (WDC) for Geomagnetism. [Dataset]. Retrieved from https://wdc.kugi.kyoto-u.ac.jp/wdc/Sec3.html

Wu, Z., Su, Z., Goldstein, J., Liu, N., He, Z., Zheng, H., & Wang, Y. (2022). Nightside plasmaspheric plume-to-core migration of whistler-mode hiss waves. *Geophysical Research Letters*, *49*(16), e00306. https://doi.org/10.1029/2022GL100306

Wygant, J. R. (2022). Van Allen Probe A DC-coupled EFW 1-second sensor potentials relative to spacecraft in volts [Dataset]. NASA Space Physics Data Facility. https://doi.org/10.48322/7mwt-de58

Wygant, J. R., Bonnell, J. W., Goetz, K., Ergun, R. E., Mozer, F. S., Bale, S. D., et al. (2013). The electric field and waves instruments on the radiation belt storm probes mission. *Space Science Reviews*, *179*(1–4), 183–220. https://doi.org/10.1007/s11214-013-0013-7

Xiao, F., Su, Z., Zheng, H., & Wang, S. (2009). Modeling of outer radiation belt electrons by multidimensional diffusion process. *Journal of Geophysical Research*, *114*(A3), A03201. https://doi.org/10.1029/2008JA013580

Yang, L., Li, L., Cao, J., & Yu, J. (2022). Statistical properties of whistler-mode hiss waves in the inner radiation belt. *Journal of Geophysical Research: Space Physics*, *127*(5), e30444. https://doi.org/10.1029/2022JA030444

Yu, J., Li, L. Y., Cao, J. B., Chen, L., Wang, J., & Yang, J. (2017). Propagation characteristics of plasmaspheric hiss: Van Allen Probe observations and global empirical models. *Journal of Geophysical Research: Space Physics*, *122*(4), 4156–4167. https://doi.org/10.1002/2016JA023372

Zhang, W., Ni, B., Huang, H., Summers, D., Fu, S., Xiang, Z., et al. (2019). Statistical properties of hiss in plasmaspheric plumes and associated scattering losses of radiation belt electrons. *Geophysical Research Letters*, *46*(11), 5670–5680. https://doi.org/10.1029/2018GL081863

Zhao, H., Ni, B., Li, X., Baker, D. N., Johnston, W. R., Zhang, W., et al. (2019). Plasmaspheric hiss waves generate a reversed energy spectrum of radiation belt electrons. *Nature Physics*, *15*(4), 367–372. https://doi.org/10.1038/s41567-018-0391-6

Zhou, Q., Xiao, F., Yang, C., Liu, S., He, Y., Wygant, J. R., et al. (2016). Evolution of chorus emissions into plasmaspheric hiss observed by Van Allen Probes. *Journal of Geophysical Research: Space Physics*, *121*(5), 4518–4529. https://doi.org/10.1002/2016JA022366

Zhu, H., Su, Z., Xiao, F., Zheng, H., Wang, Y., Shen, C., et al. (2015). Plasmatrough exohiss waves observed by Van Allen Probes: Evidence for leakage from plasmasphere and resonant scattering of radiation belt electrons. *Geophysical Research Letters*, *42*(4), 1012–1019. https://doi.org/10.1002/2014GL062964

Zudin, I. Y., Zaboronkova, T. M., Gushchin, M. E., Aidakina, N. A., Korobkov, S. V., & Krafft, C. (2019). Whistler waves' propagation in plasmas with systems of small-scale density irregularities: Numerical simulations and theory. *Journal of Geophysical Research: Space Physics*, *124*(6), 4739–4760. https://doi.org/10.1029/2019JA026637